

A fast and reliable method for the comparison of covariance matrices

Tassia Ferreira^{1,2} and Valerio Marra^{2,3,4,5}

¹*PPG Cosmo, Universidade Federal do Espírito Santo, 29075-910, Vitória, ES, Brazil*

²*Laboratório Interinstitucional de e-Astronomia - LIneA, 20921-400, Rio de Janeiro, RJ, Brazil*

³*Núcleo de Astrofísica e Cosmologia & Departamento de Física, Universidade Federal do Espírito Santo, 29075-910, Vitória, ES, Brazil*

⁴*INAF – Osservatorio Astronomico di Trieste, via Tiepolo 11, 34131, Trieste, Italy*

⁵*IFPU – Institute for Fundamental Physics of the Universe, via Beirut 2, 34151, Trieste, Italy*

Accepted XXX. Received YYY; in original form ZZZ

ABSTRACT

Covariance matrices are important tools for obtaining reliable parameter constraints. Advancements in cosmological surveys lead to larger data vectors and, consequently, increasingly complex covariance matrices, whose number of elements grows as the square of the size of the data vector. The most straightforward way of comparing these matrices involve a full cosmological analysis, which can be very computationally expensive. Using the concept and construction of compression schemes, which have become increasingly popular, we propose a fast and reliable way of comparing covariance matrices. The basic idea is to only focus on the portion of the covariance matrix that is relevant for the parameter constraints and quantify, via a fast Monte Carlo simulation, the difference of a second candidate matrix from the baseline one. To test this method, we applied it to two covariance matrices that were used to analyse the cosmic shear measurements for the Dark Energy Survey. We found that the uncertainties on the parameters change by 2.6%, a figure in qualitative agreement with the full cosmological analysis. While our approximate method cannot replace a full analysis, it may be useful during the development and validation of codes that estimate covariance matrices. Our method takes roughly 100 times less CPUh than a full cosmological analysis.

Key words: cosmology: observations–cosmological parameters–methods: statistical

1 INTRODUCTION

Cosmology has entered its golden era, with the fast advancement of technology allowing us to build telescopes capable of exploring almost the entire observable universe. As we brace ourselves for the unprecedented amount of data that will be made available in upcoming surveys like J-PAS,¹ LSST,² Euclid³ and SKA,⁴ we must tackle the issue of how to process and extract as much information as possible from the data.

This brings us to the issue of software development and validation (see, e.g., Chisari et al. 2019; Blanchard et al. 2020). Here, we discuss covariance matrix validation, which, to our knowledge, has not yet been systematically investigated. Covariance matrices are important pieces to the

puzzle as they take into consideration not only the statistical and systematic errors of the measurement, but also the correlation between each quantity. The size of a covariance matrix grows as the square of the size N of the dataset, which makes them increasingly harder to obtain, whether analytically or through simulations. Further, analysing and comparing them also becomes exceedingly difficult.

The most certain and forward way of comparing covariance matrices is in terms of their ability to reproduce cosmology, that is, by performing a full Bayesian analysis. Performing this analysis for every new covariance matrix, however, is very time consuming and computationally expensive. In this work, we seek a fast way of comparing them that eliminates the need for a cosmological analysis. The motivation is simple: if two covariance matrices produce similar results, then they should, at some level, have comparable features. We find here that even matrices with elements differing by several orders of magnitude (both diagonal and off-diagonal terms) produce parameter estimates that are almost indistinguishable from each other. It is, therefore,

¹ www.j-pas.org

² www.lsst.org

³ www.euclid-ec.org

⁴ www.skatelescope.org

conceivable to think that a fair comparison cannot rely on the elements of the full covariance matrix. In [Ferreira et al. \(2021\)](#) one of the highlighted results is the potential in using compressed covariance matrices for comparison. It is shown that two different compressed covariance matrices with consistent parameter constraints also show good agreement in a one-to-one element comparison.

Compression methods are powerful tools for reducing the dimensionality of the covariance matrix in order to facilitate and potentially speed up the process of parameter estimation. The most successful compression schemes are capable of taking a covariance matrix of size $N \times N$ and shrinking it down to $n \times n$, where n is the number of free parameters. In this work, we use the Massively Optimised Parameter Estimation and Data compression algorithm (MOPED), as described by [Heavens et al. \(2000\)](#), which works remarkably well in the case of Gaussian data, where only the mean depends on the parameters. When these circumstances are met, the method is said to be lossless in the sense that there is no loss of precision in the parameter constraints.

On the other hand, compression schemes are non-invertible, which means that, given a compressed matrix, we are unable to return to the original covariance matrix. In this sense, even if we were able to obtain a compressed covariance matrix, either analytically or with simulations, we would have no way of applying it to our real dataset of interest.

Here, we develop a method to recreate the full matrix given a compressed one. Furthermore, we propose a fast and reliable method to compare compressed covariance matrices that discards the need for a full cosmological analysis.

This paper is organised as follows. In Section 2, we review the matrix compression method we adopt, while we discuss in Section 3 invertible compression. We present our method to compare covariance matrices in Section 4, where we also analyse two cosmic shear covariance matrices. We conclude in Section 5.

2 COMPRESSION SCHEME

Consider a dataset represented by the vector $\mathbf{x} = (x_1, x_2, \dots, x_N)$ with probability distribution $L(\mathbf{x}; \Theta)$, where $\Theta = (\theta_1, \theta_2, \dots, \theta_n)$ is a vector of the model parameters. Take the logarithm of the probability distribution, $\mathcal{L} = \ln L$; its first derivative, $\mathcal{L}_{,i}$, known as the score function, tells how sensitive the model is with respect to the parameters. Its second derivative, the Hessian matrix,

$$\mathbf{H}_{ij} = \mathcal{L}_{,ij} , \quad (1)$$

describes the correlation of the estimated values of θ_i and θ_j . The expectation value of the negative of the Hessian, $\mathbf{F}_{ij} = -\langle \mathbf{H}_{ij} \rangle$, gives us the Fisher information matrix, which is an essential quantity in Bayesian statistics and, as we will see, for compressing covariance matrices. To obtain a compression scheme capable of retaining the highest amount of information, we seek to maximise \mathbf{F}_{ij} ; to do so, we start with the log-likelihood function for a Gaussian probability

distribution,⁵

$$2\mathcal{L} = \ln \det \mathbf{C} + (\mathbf{x} - \boldsymbol{\mu})^t \mathbf{C}^{-1} (\mathbf{x} - \boldsymbol{\mu}) , \quad (2)$$

with both the covariance matrix, $\mathbf{C} = \langle (\mathbf{x} - \boldsymbol{\mu})(\mathbf{x} - \boldsymbol{\mu})^t \rangle$, and $\boldsymbol{\mu} = \langle \mathbf{x} \rangle$ dependent of the model parameters Θ . We also define the data matrix as

$$\mathbf{D} \equiv (\mathbf{x} - \boldsymbol{\mu})(\mathbf{x} - \boldsymbol{\mu})^t . \quad (3)$$

Taking this definition and using $\ln \det \mathbf{C} = \text{Tr} [\ln \mathbf{C}]$, we can express Eq. (2) in a simpler form,

$$2\mathcal{L} = \text{Tr} \left[\ln \mathbf{C} + \mathbf{C}^{-1} \mathbf{D} \right] . \quad (4)$$

Derivating for θ_i and θ_j , we find the quantity we wish to maximize:

$$\langle \mathcal{L}_{,ij} \rangle = \frac{1}{2} \text{Tr} \left[\mathbf{C}^{-1} \mathbf{C}_{,i} \mathbf{C}^{-1} \mathbf{C}_{,j} + \mathbf{C}^{-1} \mathbf{M}_{ij} \right] , \quad (5)$$

where $\mathbf{M}_{ij} = \boldsymbol{\mu}_{,i} \boldsymbol{\mu}_{,j}^t + \boldsymbol{\mu}_{,j} \boldsymbol{\mu}_{,i}^t$.

There are three ways one can proceed from here, with respect to the dependence on the model parameters: 1) there is the more general case, where both the mean and the covariance depend on the model parameters; 2) only the covariance has a dependence, in which case the second term vanishes; and 3) only the mean is dependent, and the first term vanishes. The general case has been tackled by [Alsing & Wandelt \(2018\)](#), where they use the score function to derive n compressed statistics of the data. The second case often reduces to a Karhunen-Loève eigenvalue problem that results in keeping only the linear combinations of the data with the most informative eigenvalues ([Alonso 2018](#)). Finally, the third case is the basis for MOPED ([Tegmark et al. 1997](#); [Heavens et al. 2000](#)), which uses linear compression to radically reduce the dataset. Here, we will only be working with the latter, with an extension for other compression methods being planned for future works. In this case, Eq. (5) reduces to

$$\mathbf{F}_{ij} = \langle \mathcal{L}_{,ij} \rangle = \frac{1}{2} \text{Tr} \left[\mathbf{C}^{-1} \mathbf{M}_{ij} \right] . \quad (6)$$

For the simplest case of only one parameter, we have

$$\mathbf{F}_{11} = \boldsymbol{\mu}_{,1}^t \mathbf{C}^{-1} \boldsymbol{\mu}_{,1} . \quad (7)$$

If we apply a compression of the type $y = \mathbf{b}^t \mathbf{x}$, we can follow these same steps to obtain the compressed Fisher matrix,

$$\mathbf{F}_{11}^{\text{comp}} = \frac{\mathbf{b}^t \mathbf{M}_{11} \mathbf{b}}{\mathbf{b}^t \mathbf{C} \mathbf{b}} . \quad (8)$$

To find an extremum such that $\mathbf{b}^t \mathbf{C} \mathbf{b} = 1$, we apply a Lagrange multiplier,

$$\boldsymbol{\mu}_{,1} (\mathbf{b}^t \boldsymbol{\mu}_{,1}) = \lambda \mathbf{C} \mathbf{b} . \quad (9)$$

The solution is the eigenvector which, when normalised, gives

$$\mathbf{b}_1 = \frac{\mathbf{C}^{-1} \boldsymbol{\mu}_{,1}}{\sqrt{\boldsymbol{\mu}_{,1}^t \mathbf{C}^{-1} \boldsymbol{\mu}_{,1}}} . \quad (10)$$

Plugging this back in Eq. (8), we find

$$\mathbf{F}_{11}^{\text{comp}} = \boldsymbol{\mu}_{,1}^t \mathbf{C}^{-1} \boldsymbol{\mu}_{,1} = \mathbf{F}_{11} , \quad (11)$$

⁵ We have dropped the additive constant $n \ln(2\pi)$.

which shows that the Fisher matrix is unchanged.

We can further expand Eq. (10) to multiple parameters. By employing a Gram-Schmidt decomposition, we obtain y_i 's that are orthonormal, uncorrelated and carry as much information as possible about the parameter θ_i . We then have,

$$\mathbf{b}_n = \frac{\mathbf{C}^{-1}\boldsymbol{\mu}_{,n} - \sum_{q=1}^{n-1} (\boldsymbol{\mu}_{,n}^t \mathbf{b}_q) \mathbf{b}_q}{\sqrt{\boldsymbol{\mu}_{,n}^t \mathbf{C}^{-1} \boldsymbol{\mu}_{,n} - \sum_{q=1}^{n-1} (\boldsymbol{\mu}_{,n}^t \mathbf{b}_q)^2}}, \quad (12)$$

for $q < n$. With this in hand, the resulting weighing matrix \mathbf{b} contains n rows, and the covariance matrix is shrunk to $n \times n$.

To use MOPED as described here, we have assumed a Gaussian likelihood and that the fiducial value at which the derivatives are taken are those at the maximum likelihood point. If one does not have prior knowledge of this value, then one could iterate to find it but, as Heavens et al. (2000) have found, this is often unnecessary. We also trust that the cosmological model we have chosen is the correct one; deviations from a baseline cosmological model can be accounted for by introducing additional weighing vectors, as described in Heavens et al. (2020).

3 INVERTIBLE COMPRESSION

The next step in our analysis is to obtain an invertible transformation, based on the compression scheme we have found, that is able to reproduce the same parameter constraints we previous obtained with both the original and the compressed covariance matrices. Here, we will not be reducing the size of the covariance matrix, but rather the number of relevant elements. To do so, we start with the non-normalized Eq. (10), and expand it to an invertible, $n \times n$ transformation matrix,

$$\mathbf{B} = (\mathbf{b} \ U), \quad (13)$$

where U has dimension $(N - n) \times N$. We want to find U such that

$$\mathbf{C}^{\text{trans}} = \mathbf{B}^t \mathbf{C} \mathbf{B} = \begin{pmatrix} \mathbf{b}^t \mathbf{C} \mathbf{b} & 0 \\ 0 & U \mathbf{C} U^t \end{pmatrix}, \quad (14)$$

which implies

$$\mathbf{b}^t \mathbf{C} U = 0. \quad (15)$$

For the above to be true, the rows of U must be composed of vectors which form the nullspace of $\mathbf{b}^t \mathbf{C}$. To simplify notation, we represent the transformed covariance matrix, partitioned blockwise as,

$$\begin{pmatrix} C1 & 0 \\ 0 & C3 \end{pmatrix}. \quad (16)$$

In the following Section, we apply this transformation to a toy example, so we can explore, in a more didactic manner, how this transformation alters the covariance matrix.

3.1 Toy example

In order to better understand our invertible transformation and how $C3$ affects \mathbf{C} , we take a simple toy example. Con-

sider the Gaussian data described by:

$$\{t_i, x_i\} \text{ with } i = 1, 2, 3, \\ C = \sigma^2 I_3, \quad (17)$$

where I_3 is the 3-d identity matrix and t_i is the independent variable associated to x_i . Next, we propose the following model:

$$\mu(t) = \theta_1 + \theta_2 t, \quad (18)$$

for which we can obtain the likelihood as

$$2\mathcal{L} = (x_i - \mu(t_i)) C_{ij}^{-1} (x_j - \mu(t_j)) \\ = \sum_{i=1,2,3} \frac{(x_i - \mu(t_i))^2}{\sigma^2}. \quad (19)$$

The next step is then to derive an explicit expression for \mathbf{b} , U , $C1$ and $C3$ as a function of t_i , x_i , σ and θ_i . We start with

$$\mathbf{b} = \begin{pmatrix} \frac{1}{\sigma^2} & \frac{1}{\sigma^2} & \frac{1}{\sigma^2} \\ \frac{t_1}{\sigma^2} & \frac{t_2}{\sigma^2} & \frac{t_3}{\sigma^2} \end{pmatrix} \quad (20)$$

and

$$U = \begin{pmatrix} -\frac{t_2+t_3}{t_1-t_2} & -\frac{t_1-t_3}{t_1-t_2} & 1 \end{pmatrix}, \quad (21)$$

which we can use to find,

$$\mathbf{C}^{\text{trans}} = \begin{pmatrix} \frac{3}{\sigma^2} & \frac{t_1+t_2+t_3}{\sigma^2} & 0 \\ \frac{t_1+t_2+t_3}{\sigma^2} & \frac{t_1^2+t_2^2+t_3^2}{\sigma^2} & 0 \\ 0 & 0 & \mathbf{C3} \end{pmatrix}, \quad (22)$$

where

$$\mathbf{C3} = 2\sigma^2 \frac{t_1^2 + t_2^2 + t_3^2 - t_2 t_3 - t_1(t_2 + t_3)}{(t_1 - t_2)^2}. \quad (23)$$

Plugging our values in Eq. (6), we get,

$$F_{ij}^{\text{trans}} = \begin{pmatrix} \frac{3}{\sigma^2} & \frac{t_1+t_2+t_3}{\sigma^2} \\ \frac{t_1+t_2+t_3}{\sigma^2} & \frac{t_1^2+t_2^2+t_3^2}{\sigma^2} \end{pmatrix} = C1. \quad (24)$$

Making $\mathbf{C3} = C3$, we can revert back the transformation to find C' . If we substitute C' in Eq. (6), we find that $F' = F$, which shows that the Fisher matrix of the modified covariance matrix does not depend on $C3$.

3.2 Cosmic shear example

Light from distant galaxies is deflected by the gravitational field of large-scale structures as it travels through the Universe. This creates a correlated distortion of images, known as cosmic shear, which can be used to directly probe the underlying dark matter distribution, providing insight into the growth of structures and the geometry of the Universe. Cosmic shear has thus emerged as a powerful probe for dark energy (Kilbinger 2015). We review cosmic shear statistics in Appendix A.

3.2.1 The DESY1 data

The cosmic shear measurements for the Year 1 release of the Dark Energy Survey, (DESY1, Troxel et al. 2018),

were taken over an area of 1321 deg² of the southern sky and are divided into four tomographic redshift bins from $0.20 < z < 1.30$ (Zuntz et al. 2018), according to the posterior of the photometric redshift as estimated from *griz* flux measurements (Hoyle et al. 2018).

Each of the 10 bin-pair combinations contains 20 angular bins between 2.5 and 250 arcmin, yielding a data vector of length 200, for each statistic. Not all angular bins are used however, due to cuts that remove angular scales sensitive to baryonic effects, thus reducing the data vector to 167 points for $\xi_+(\theta)$ and 67 for $\xi_-(\theta)$, totalling 227 points.

We assume a flat Λ CDM model, with six free parameters, $\{A_s, \Omega_m, \Omega_b, \Omega_\nu h^2, H_0, n_s\}$, and fix $w = -1$ and $\tau = 0.08$. Since we disconsider the baryonic effects, the astrophysical systematics are largely dominated by intrinsic alignment (IA), which describes the coherent orientation of galaxies due to overdense regions. We vary the amplitude of the nonlinear alignment model, A_{IA0} , and its redshift evolution, η_{IA} , which are related via $A_{IA0} \equiv A_{IA0} [(1+z)/(1+z_0)]^{\eta_{IA}}$, where $z_0 = 0.62$ is the pivot redshift. We also have the shear multiplicative bias, given by

$$\xi^{ij} = (1 + m^i)(1 + m^j) \xi_{\text{true}}^{ij}, \quad (25)$$

where m^i varies with each tomographic bin. Lastly, we vary the photo- z bias, Δz^i , on the distribution of galaxies in each redshift bin, $n^i(z)$, as described by

$$n^i(z) = n_{PZ}^i (z - \Delta z^i). \quad (26)$$

The priors for these 16 parameters are given in Table 1. For brevity, we show the probability density functions (PDFs) only for the matter density parameter Ω_m and the amplitude of matter fluctuations $S_8 \equiv \sigma_8(\Omega_m/0.3)^{0.5}$.

Finally, the parameter constraints are obtained with CosmoSIS (Zuntz et al. 2015), while employing the MultiNest (Feroz et al. 2009) sampler and following the same pipeline described in Troxel et al. (2018), with the modified likelihood for the transformed and compressed datasets and covariance matrices used in Ferreira et al. (2021). The MultiNest settings had 1000 livepoints, efficiency set to 0.05, tolerance to 0.1 and constant efficiency set to True.

3.2.2 The KiDS-1000 data

The measurements for the Kilo-Degree Survey 1000 (KiDS-1000, Asgari et al. 2021) contain 1006 deg² of images, with the primary images taken in the r -band, but with the final set having photometry in *ugriZYJHK_s* (Wright et al. 2019), after being combined with infrared data from the VISTA Kilo-degree INfrared Galaxy survey (VIKING, Edge et al. (2013)). The data is divided into five tomographic bins, z_B , based on their best-fitting photometric redshifts and ranging from $0.1 < z < 1.2$.

There are nine angular bins between 0.5 and 500 arcmin, resulting in a data vector of length 270. The angular cuts are applied to $\xi_-(\theta)$, removing scales with $\theta < 4$ arcmin (Hildebrandt et al. 2017), which leaves 135 data points for $\xi_+(\theta)$ and 90 for $\xi_-(\theta)$. The final dataset has length 235, with a 235×235 covariance matrix.

Similarly to the DESY1 analysis, we take a flat Λ CDM

Parameter	Prior
Cosmological	
Ω_m	$\mathcal{U}(0.1, 0.9)$
$\log A_s$	$\mathcal{U}(3.0, 3.1)$
H_0 (km s ⁻¹ Mpc ⁻¹)	$\mathcal{U}(55, 91)$
Ω_b	$\mathcal{U}(0.03, 0.07)$
$\Omega_\nu h^2$	$\mathcal{U}(0.0005, 0.01)$
n_s	$\mathcal{U}(0.87, 1.07)$
Astrophysical	
A_{IA0}	$\mathcal{U}(-5, 5)$
η_{IA}	$\mathcal{U}(-5, 5)$
Systematic	
m^i	$\mathcal{G}(0.012, 0.023)$
Δz^1	$\mathcal{G}(-0.001, 0.016)$
Δz^2	$\mathcal{G}(-0.019, 0.013)$
Δz^3	$\mathcal{G}(0.009, 0.011)$
Δz^4	$\mathcal{G}(-0.018, 0.022)$

Table 1. List of the priors used in the analysis for parameter constraints using the dataset described in §3.2.1. \mathcal{U} denotes flat in the given range and \mathcal{G} is Gaussian with mean equal to its first argument and dispersion equal to its second.

model, with $w = -1$, and five free cosmological parameters, $\{S_8, \Omega_c h^2, \Omega_b h^2, h, n_s\}$. There are two astrophysical nuisance parameters: the baryon feedback parameter, A_{bary} and A_{IA} , where, for analyses with this dataset, the latter does not carry a redshift dependence. The mean of the five redshift distributions is also allowed to vary and are correlated through their covariance matrix. Finally, for the analyses with $\xi_+(\theta)$, we have,

$$\delta_c = \pm \sqrt{c_1^2 + c_2^2}, \quad (27)$$

to account for the uncertainty of the additive ellipticity bias terms, c_1 and c_2 , assuming that they are constants. Table 2 shows the parameters varied as well as their priors.

For parameter constraints, we use the MultiNest sampler within CosmoSIS, with the same settings described in the previous section, but with the KiDS Cosmology Analysis Pipeline, KCAP (Asgari et al. 2021). We use a modified likelihood to account for the transformed and compressed covariance matrices and data vectors.

3.2.3 The covariance matrices

There are three distinct covariance matrices used in this work, which will be described in this section. What we refer to as the *DES Covariance Matrix* (DCM), throughout the text is the DESY1 cosmic shear covariance matrix obtained with CosmoLike (Krause & Eifler 2017). The covariance is largely dominated by the shape-noise and Gaussian components of the covariance, with a halo model framework being used to include the non-Gaussian parts.

The second and third covariance matrices were both calculated with the code used for the KiDS-450 and KiDS-1000 surveys (Köhlinger et al. 2017; Joachimi et al. 2020). Both are calculated analytically and follow the procedure in Joachimi et al. (2008) for obtaining second-order cosmic shear measurements under the assumption that density field is Gaussian, the galaxies are uniformly distributed, and the survey has a straightforward geometry.

Parameter	Prior
Cosmological	
S_8	$\mathcal{U}(0.1, 1.3)$
$\Omega_c h^2$	$\mathcal{U}(0.051, 0.255)$
$\Omega_b h^2$	$\mathcal{U}(0.019, 0.026)$
h	$\mathcal{U}(0.64, 0.82)$
n_s	$\mathcal{U}(0.84, 1.1)$
Astrophysical	
A_{IA}	$\mathcal{U}(-6, 6)$
A_{bary}	$\mathcal{U}(2.0, 3.13)$
Systematic	
δ_{SN}^1	$\mathcal{G}(0, 1.0)$
δ_{SN}^2	$\mathcal{G}(-0.181, 1.0)$
δ_{SN}^3	$\mathcal{G}(-1.110, 1.0)$
δ_{SN}^4	$\mathcal{G}(-1.395, 1.0)$
δ_{SN}^5	$\mathcal{G}(1.265, 1.0)$
δ_c	$\mathcal{G}(0, 2.3 \times 10^{-4})$

Table 2. List of the priors used in the analysis for parameter constraints using the dataset described in §3.2.2.

The one which we label the *Gaussian Covariance Matrix* (GCM) constitutes of only the Gaussian contributions to shape-noise, sample variance and the mixed noise-sample variance term. We do not include the non-Gaussian components and the super-sample covariance so that the differences are accentuated in the two covariance matrices and in the parameter constraints. This covariance matrix is used here along with the DCM to test our algorithm for comparing covariance matrices. It has been shown in Ferreira et al. (2021) that their parameter constraints are accurately reproduced when compressed with MOPED.

Finally, the *KiDS Covariance Matrix* (KCM) is the one we use for testing our invertible transformation as well as for some of the tests with $C3$. It is the same covariance matrix used in the KiDS-1000 survey analysis with cosmic shear, and it has two additional terms, as compared to GCM. One of them is responsible for the non-Gaussianity of the field, which generates higher-order correlations between different modes, and the other for the super-sample covariance, which accounts for these correlations between modes in the survey and those that are larger than the survey scale.

3.2.4 Perturbing $C3$

We now perturb the $C3$ in a given fashion and perform a full cosmological analysis with the perturbed covariance matrix to see the impact on the parameter constraints. We start with the simple task of making $C3 = \mathbb{1}$. This modification increases the diagonal elements by several orders of magnitude and negates all the cross terms of $C3$. Fig. 1 shows, in the case of KCM, that the constraints are consistent with the unmodified covariance matrix, showing that this configuration is irrelevant for the parameter constraints.

To verify that this is not a particular case, we perturb the elements of the $C3$ block of DCM by introducing a Gaussian error of 5%, 10% and 50%. The size of the 2σ constraints of Ω_m and S_8 are basically identical to those obtained with the unperturbed, transformed covariance matrix, see Fig. 2 (top panel).

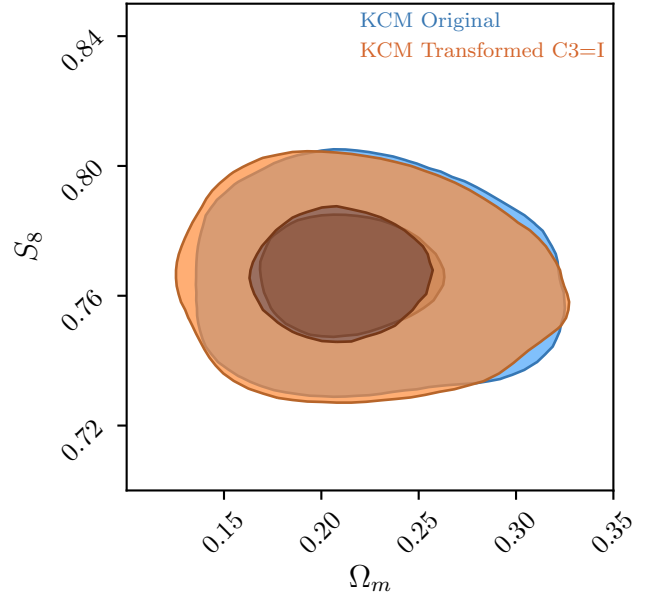


Figure 1. KiDS-1000 parameter constraints for the original and transformed covariance matrix for the cosmological parameters Ω_m and S_8 . The darker curve, in blue, is for the original covariance matrix and the lighter curve, in orange, is for when the block $C3$ of KCM is replaced by the identity matrix.

The next question to address is how this property propagates when we apply the inverse of the transformation \mathbf{B} to the perturbed $\mathbf{C}^{\text{trans}}$. We carry out the same procedure for perturbing the elements of $C3$ by 5%, 10% and 50%. We then apply \mathbf{B}^{-1} to transform it into the space of the original data vector. As expected, the results are similar to those found in the previous analysis, see Fig. 2 (bottom panel).

Finally, in Fig. 3 (left for DCM and right for KCM) we show the ratio between the elements of the perturbed covariance matrices and the original one for a 5% (top) and 50% perturbation (bottom), and highlight the diagonal elements in red. A clear trend can be seen: the smallest elements show a greater disagreement, and this decreases as their values increase. It is interesting to see that the large differences between the elements does not impact the parameter constraints, which shows that metrics to compare covariance matrices based solely on the elements themselves do not produce conclusive results. As such, our best choice is to concentrate on $C1$.

4 COMPARING COVARIANCE MATRICES

We have seen in the previous section that the relevant information for parameter constraints is contained in $C1$. This is fortunate, for comparing matrices, because we can reduce the dimensionality of large covariance matrices. In this section we explain the method we have developed for obtaining a reliable metric of comparison that discards the need for a full cosmological analysis.

Take two covariance matrices: the one we are testing against, C_{base} , and the one we want tested, C_{test} . First, we obtain the corresponding $C1$ blocks as explained earlier.

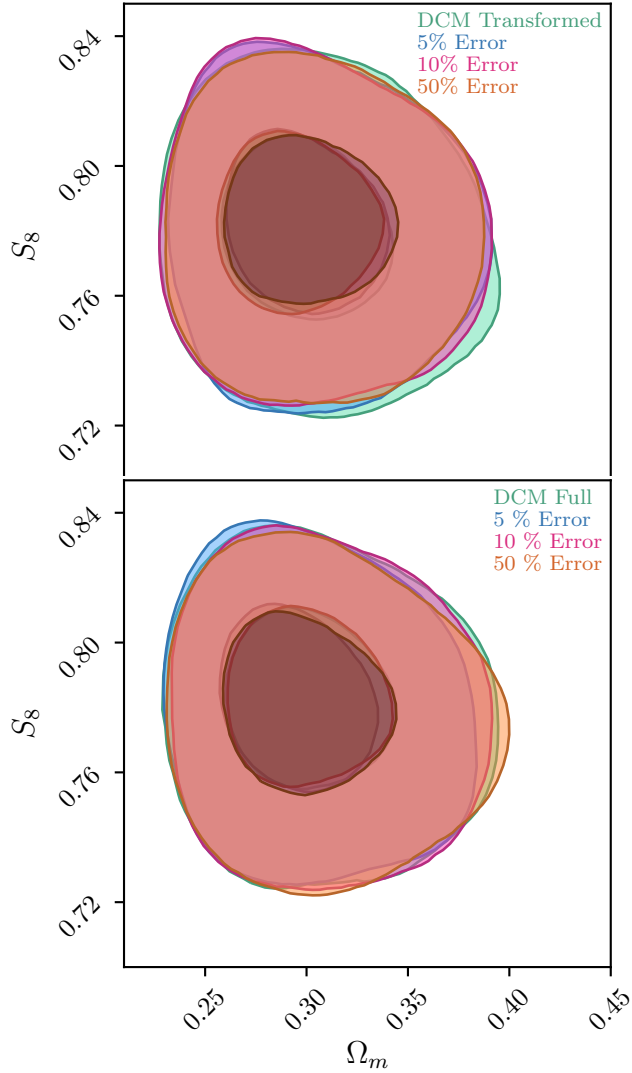


Figure 2. *Top:* DESY1 constraints on Ω_m and S_8 for the transformed covariance matrix (green) and for a 5% (blue), 10% (pink) and 50% (orange) perturbation applied to the $C3$ block of DCM. *Bottom:* DESY1 constraints for the original covariance matrix (green) and for three covariance matrices produced by applying the inverse transformation to those with 5% (blue), 10% (pink) and 50% (orange) perturbation applied to the $C3$ block of the transformed DCM.

Then, we divide the comparison into two parts: analysis of the diagonal elements of $C1$, the n -dimensional vector \mathcal{D} , and of the independent elements of the correlation matrix relative to $C1$, the $n(n-1)/2$ -dimensional vector \mathcal{C} .

We developed a comprehensible code in python⁶ that uses the following procedure to test \mathcal{D} and \mathcal{C} :

- (i) create a mock sample $\{\mathcal{D}_{\delta,i}\}$ by perturbing, with a given error percentage δ , the vector $\mathcal{D}_{\text{base}}$ (or $\mathcal{C}_{\text{base}}$);
- (ii) produce the sample covariance matrix S_δ from the gen-

erated mocks:

$$S_\delta = \frac{1}{m-1} \sum_{i=1}^m (\mathcal{D}_{\delta,i} - \overline{\mathcal{D}_\delta}) (\mathcal{D}_{\delta,i} - \overline{\mathcal{D}_\delta})^t,$$

where m is the size of the mock sample;

- (iii) obtain the fiducial χ^2 -distribution using:

$$\chi_{\delta,i}^2 = (\mathcal{D}_{\delta,i} - \mathcal{D}_{\text{base}}) S_\delta^{-1} (\mathcal{D}_{\delta,i} - \mathcal{D}_{\text{base}})^t;$$

- (iv) calculate $\chi_{\text{test}}^2 = (\mathcal{D}_{\text{test}} - \mathcal{D}_{\text{base}}) S_\delta^{-1} (\mathcal{D}_{\text{test}} - \mathcal{D}_{\text{base}})^t$;
- (v) find $\delta_{\text{test}}^{\mathcal{D}}$ such that χ_{test}^2 is the maximum of the χ^2 -distribution above;
- (vi) find $\sigma_\delta = (\delta_+ - \delta_-)/2$, where δ_+ is the value that makes χ_{test}^2 fall at the right-hand border of the 68% probability interval of the χ^2 -distribution, and similarly for δ_- .

The value of $\delta_{\text{test}}^{\mathcal{D}} \pm \sigma_\delta$ found by this method estimates the distance between the two $C1$ matrices, C_{base} and C_{test} , as far as the uncertainties or correlations in the parameters are concerned.

We now explain how we perturb $\mathcal{D}_{\text{base}}$ and $\mathcal{C}_{\text{base}}$. For the diagonal part, the mocks were generated by drawing $\mathcal{E}_{\mathcal{D}}$ from a multivariate Gaussian distribution $\mathcal{G}[0_n, \delta^2 I_n]$, such that,

$$\mathcal{D}_{\delta,i} = (1 + \mathcal{E}_{\mathcal{D}}) \mathcal{D}_{\text{base}}. \quad (28)$$

In the case of the correlation matrix, we encounter the restriction that the values must be in the range $[-1, 1]$. Applying this by force could result in a perturbation not cohesive with our chosen δ . We resolve this by working with the hyperbolic tangent function and correcting for the Jacobian,

$$z_i = \tanh^{-1}(\mathcal{C}_{\text{base}}), \quad (29)$$

$$\delta z_i = \mathcal{E}_{\mathcal{C}} \left[\cosh \left(z_i + \frac{1}{2} \mathcal{E}_{\mathcal{C}} \right) \right]^2,$$

where $\mathcal{E}_{\mathcal{C}}$ is drawn similarly to $\mathcal{E}_{\mathcal{D}}$. Our perturbed vector then becomes,

$$\mathcal{C}_{\delta,i} = \tanh(z_i + \delta z_i). \quad (30)$$

For steps (v-vi), we use `lmfit`'s minimize function and define the default to use Powell's method. For the mocks, we take the sample size m to be 1000. This returns a value of δ_{test} in a few minutes, but, for robustness, we recommend setting this to > 5000 .

4.1 Cosmic shear covariance matrices

We test this method by comparing the DCM and GCM covariance matrices. The full Bayesian analysis of Fig. 4 shows that the two matrices give similar constraints, with the constraints relative to DCM a little weaker than the ones relative to GCM. More precisely, in the 16-dimensional parameter space, the volume of the posterior is about 20% smaller for the latter. In terms of constraints for individual parameters, the percentage differences for the cosmological parameters are up to 1.2%, with the interval shifts for the 68% contour levels of 2.4%, with larger differences for the nuisance parameters (of 6.2% and 24%, respectively).

Next we apply our fast method. We adopt $C_{\text{base}} = \text{DCM}$ and $C_{\text{test}} = \text{GCM}$. Fig. 5 shows the χ^2 -distributions used by our method: the values of δ_{test} are such that the χ_{test}^2 values

⁶ github.com/t-ferreira/Covariance_comparison

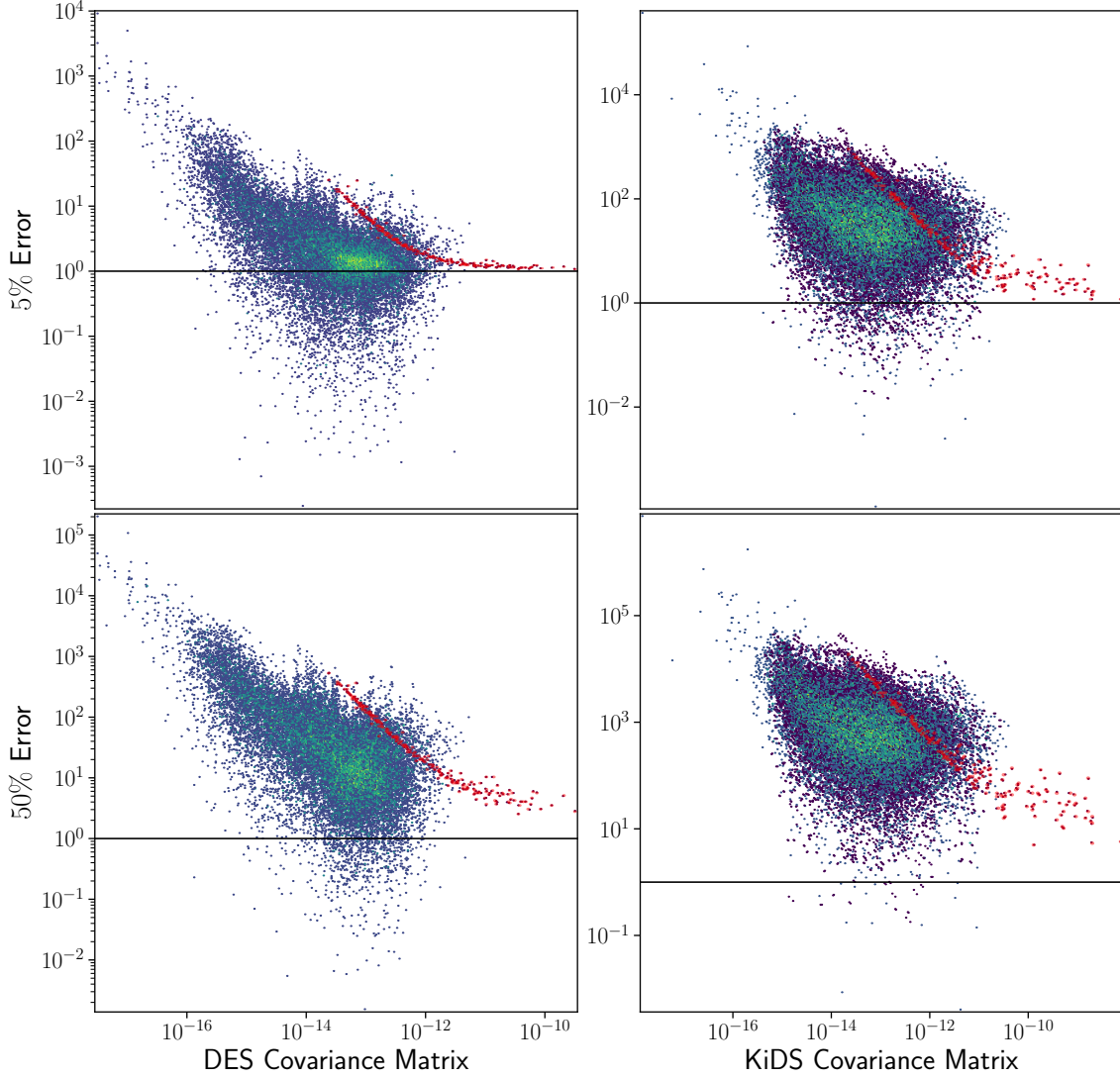


Figure 3. Scatter plots of the ratio of the elements of the perturbed covariance matrix and those of the original one against the latter. The top panels show the ratio for a 5% perturbation, the bottom ones for a 50% perturbation, the ones on the left are relative to DESY1, and the ones on the right to KiDS-1000. The red dots represent the ratio between the diagonal elements of the two matrices.

fall at the maximum of the distributions. We find that the diagonal elements of the C1 block of GCM differ by

$$\delta_{\text{test}}^{\mathcal{D}} = 2.6 \pm 0.2\% , \quad (31)$$

while the correlations differ by:

$$\delta_{\text{test}}^{\mathcal{C}} = 7.8 \pm 0.1\% . \quad (32)$$

These results agree with the ones obtained via the full Bayesian analysis above.

Finally, our algorithm took roughly 0.5 CPUh (2020

laptop) to generate the desired output, while a full cosmological analysis takes roughly 100 times more.

5 CONCLUSION

The complexity and the considerable size of covariance matrices make them increasingly difficult to analyse. Because of the vast range of values, with its own elements often differing by several orders of magnitude, it is customary to identify

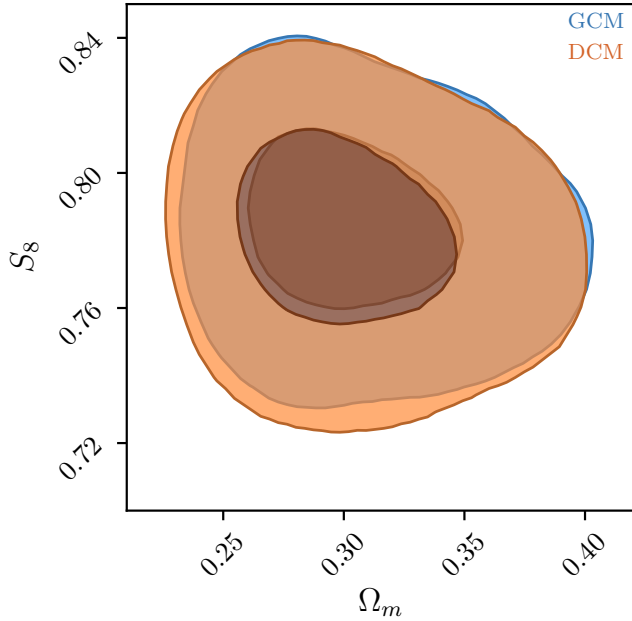


Figure 4. Constraints on the parameters Ω_m and S_8 for the DCM and GCM produced for cosmic shear, as described in §3.2.3. The orange curve is for the DCM, while the blue is for the GCM. In the 16-dimensional parameter space, the volume of the posterior is about 20% smaller for the latter.

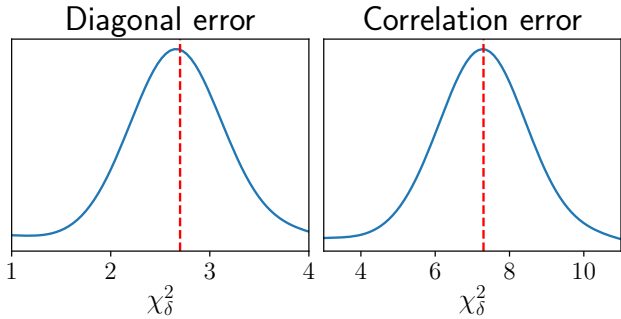


Figure 5. χ^2 -distributions that are used to determine δ_{test} for the diagonal elements of the covariance matrix (left) and for the elements of the correlation matrix (right). The method finds the δ_{test} value such that χ^2_{test} (red dashed line) falls at the maximum of the distribution.

the largest elements and the diagonal ones. Should these be similar, then it is likely that the parameter constraints are also compatible; we show here that this is a perilous assumption. Using an invertible transformation, we showed that it is possible to generate very distinct covariance matrices capable of generating the same cosmology, given the same data vector.

On the other hand, we also see that MOPED is capable of reducing the size of the covariance matrix while retaining the necessary information for parameter constraints. We use the compressed matrix formalism to develop a fast and reliable method for the comparison of covariance matrices that only considers the portion of the covariance matrix

that is relevant for the parameter constraints. Together with this work we release a comprehensible implementation in python of this method, which is available at github.com/tferreira/Covariance_comparison.

Using our method, we show that the DESY1 covariance matrix and the Gaussian covariance matrix by Joachimi et al. (2020), which produce compatible cosmological constraints, feature a difference of 7.8% for the elements of the correlation matrix and only 2.6% for the diagonal elements of the covariance matrix, in qualitative agreement with the full cosmological analysis.

While our approximate method cannot replace a full Bayesian analysis, it may be useful during the development and validation of codes that estimate covariance matrices. Our method takes roughly 100 times less CPUh than a full cosmological analysis.

ACKNOWLEDGEMENTS

It is a pleasure to thank Scott Dodelson for useful comments and discussions. TF also thanks Tilman Troester for helpful comments on how to use KCAP. TF thanks CAPES and FAPES for financial support. VM thanks CNPq and FAPES for partial financial support. This project has received funding from the European Union’s Horizon 2020 research and innovation programme under the Marie Skłodowska-Curie grant agreement No 888258.

DATA AVAILABILITY

The data underlying this article will be shared on reasonable request to the corresponding author.

References

- Alonso D., 2018, *Monthly Notices of the Astronomical Society*, 473, 4306, [1707.08950].
- Alsing J., Wandelt B., 2018, *Monthly Notices of the Royal Astronomical Society*, 476, L60, [1712.00012].
- Asgari M., et al., 2021, *Astronomy & Astrophysics*, 645, A104, [2007.15633].
- Blanchard A., et al., 2020, *Astronomy & Astrophysics*, 642, A191, [1910.09273].
- Chisari N. E., et al., 2019, *Astrophysical Journal Supplement*, 242, 2, [1812.05995].
- Edge A., Sutherland W., Kuijken K., Driver S., McMahon R., Eales S., Emerson J. P., 2013, *The Messenger*, 154, 32.
- Feroz F., Hobson M. P., Bridges M., 2009, *Monthly Notices of the Astronomical Society*, 398, 1601, [0809.3437].
- Ferreira T., Zhang T., Chen N., Dodelson S., 2021, *Physical Review D*, 103, 103535, [2010.15986].
- Heavens A., Jimenez R., Lahav O., 2000, *Monthly Notices of the Royal Astronomical Society*, 317, 965, [astro-ph/9911102].
- Heavens A. F., Sellentin E., Jaffe A. H., 2020, *Monthly Notices of the Royal Astronomical Society*, 498, 3440, [2006.06706].
- Hildebrandt H., et al., 2017, *Monthly Notices of the Astronomical Society*, 456, 1454, [1606.05338].
- Hoyle B., Gruen D., Bernstein G. M., Rau M. M., de Vicente J., et al., 2018, *Monthly Notices of the Royal Astronomical Society*, 478, 592, [1708.01532].
- Joachimi B., Schneider P., Eifler T., 2008, *Astronomy & Astrophysics*, 477, 43, [0708.0387].

- Joachimi B., Lin C. A., Asgari M., Tröster T., Heymans C., et al., 2020, *Astronomy & Astrophysics*, 646, A129, [2007.01844].
- Kilbinger M., 2015, *Reports on Progress in Physics*, 78, 086901, [1411.0115].
- Köhlinger F., et al., 2017, *Monthly Notices of the Astronomical Society*, 471, 4412, [1706.02892].
- Krause E., Eifler T., 2017, *Monthly Notices of the Astronomical Society*, 470, 2100, [1601.05779].
- Schneider P., van Waerbeke L., Mellier Y., 2002, *Astronomy & Astrophysics*, 389, 729, [0112441].
- Tegmark M., Taylor A., Heavens A., 1997, *Astrophysical Journal*, 480, 22, [astro-ph/9603021].
- Troxel M. A., et al., 2018, *Physical Review D*, D98, [1708.01538].
- Wright A. H., et al., 2019, *Astronomy & Astrophysics*, 632, A34, [1812.06077].
- Zuntz J., et al., 2015, *Astronomy and Computing*, 12, 45, [1409.3409].
- Zuntz J., et al., 2018, *Monthly Notices of the Astronomical Society*, 481, 1149, [1708.01533].

APPENDIX A: COSMIC SHEAR STATISTICS

The mapping of the light distribution of the source to image coordinates is done via the magnification tensor, which is the inverse of the Jacobian matrix,

$$\mathbf{A} = \begin{pmatrix} 1 - \kappa - \gamma_1 & -\gamma_2 \\ -\gamma_2 & 1 - \kappa + \gamma_1 \end{pmatrix}, \quad (\text{A1})$$

with κ being the isotropic decrease or increase of the observed size of the source image and the anisotropic deformation $\gamma = \gamma_1 + i\gamma_2$ being the shear. In Fourier space, these two quantities are related via

$$\tilde{\gamma}(\boldsymbol{\ell}) = \frac{(\ell_1 + i\ell_2)^2}{\ell^2} \tilde{\kappa}(\boldsymbol{\ell}) = e^{2i\beta} \tilde{\kappa}(\boldsymbol{\ell}), \quad (\text{A2})$$

where β is the polar angle of the wave vector $\boldsymbol{\ell} = (\ell_1, \ell_2)$.

The convergence can also be interpreted according to the projected matter density, with its power spectrum being associated with that of the matter density contrast, P_δ (Schneider et al. 2002). Using several approximations, such as the Limber projection, which uses only modes that lie in the plane of the sky, the small-angle approximation, and the flat-sky limit, where we replace spherical harmonics by Fourier transforms, we can write,

$$P_\kappa(\ell) = \frac{9}{4} \Omega_m^2 \left(\frac{H_0}{c} \right)^4 \int_0^{\chi_{\text{lim}}} d\chi \frac{g^2(\chi)}{a^2(\chi)} P_\delta \left(k = \frac{\ell}{f_K(\chi)}, \chi \right). \quad (\text{A3})$$

The integral goes to the limiting comoving distance of the galaxy sample, χ_{lim} , and we identify H_0 as the value of the Hubble constant today, c as the speed of light, χ as the comoving coordinate, a as the scale factor, f_K as the comoving angular distance, and the reduced shear, g , given by,

$$g = \frac{\gamma}{1 - \kappa}. \quad (\text{A4})$$

The real-space shear two-point correlation function is the main cosmic shear observable because it can be readily obtained by averaging over the multiplied ellipticities of galaxy pairs. We can decompose the shear into its tangential component, γ_t , and the cross-component, γ_\times , which are defined as

$$\gamma_t = -\text{Re}(\gamma e^{-2i\phi}), \quad \gamma_\times = -\text{Im}(\gamma e^{-2i\phi}), \quad (\text{A5})$$

where ϕ is the polar angle of the separation vector $\boldsymbol{\theta}$. The shear correlation functions are then,

$$\begin{aligned} \xi_+(\boldsymbol{\theta}) &= \langle \gamma\gamma^* \rangle(\boldsymbol{\theta}) = \langle \gamma_t\gamma_t \rangle(\boldsymbol{\theta}) + \langle \gamma_\times\gamma_\times \rangle(\boldsymbol{\theta}), \\ \xi_-(\boldsymbol{\theta}) &= \text{Re}(\langle \gamma\gamma^* \rangle(\boldsymbol{\theta}) e^{-4i\phi}) = \langle \gamma_t\gamma_t \rangle(\boldsymbol{\theta}) - \langle \gamma_\times\gamma_\times \rangle(\boldsymbol{\theta}). \end{aligned} \quad (\text{A6})$$

Its power spectrum is given by the Fourier transform of the correlation function,

$$\begin{aligned} \langle \tilde{\gamma}(\boldsymbol{\ell})\tilde{\gamma}^*(\boldsymbol{\ell}') \rangle &= (2\pi)^2 \delta_D(\boldsymbol{\ell} - \boldsymbol{\ell}') P_\kappa(\ell), \\ \langle \tilde{\gamma}(\boldsymbol{\ell})\tilde{\gamma}(\boldsymbol{\ell}') \rangle &= (2\pi)^2 \delta_D(\boldsymbol{\ell} - \boldsymbol{\ell}') e^{4i\phi} P_\kappa(\ell), \end{aligned} \quad (\text{A7})$$

with δ_D being the Dirac function and using Eq. (A2) to write $P_\kappa(\ell) = P_\gamma(\ell)$. Finally, if we choose $\boldsymbol{\theta} = (\theta, 0)$, we have,

$$\begin{aligned} \xi_+(\boldsymbol{\theta}) &= \langle \gamma(\mathbf{0})\gamma^*(\boldsymbol{\theta}) \rangle \\ &= \int \frac{d^2\ell}{(2\pi)^2} \int \frac{d^2\ell'}{(2\pi)^2} e^{i\ell'\cdot\boldsymbol{\theta}} \langle \tilde{\gamma}(\boldsymbol{\ell})\tilde{\gamma}^*(\boldsymbol{\ell}') \rangle \\ &= \int \frac{d^2\ell'}{(2\pi)^2} e^{i\ell'\cdot\boldsymbol{\theta}} \int d^2\ell \delta_D(\boldsymbol{\ell} - \boldsymbol{\ell}') P_\kappa(\ell) \\ &= \int \frac{d^2\ell}{(2\pi)^2} e^{i\ell\cdot\boldsymbol{\theta}} P_\kappa(\ell), \end{aligned} \quad (\text{A8})$$

where we make the substitution $\boldsymbol{\ell}' \rightarrow \boldsymbol{\ell}$. If we expand $\int d^2\ell = \int \ell d\ell \int d\varphi$,

$$= \int_0^\infty \frac{\ell d\ell}{(2\pi)^2} P_\kappa(\ell) \int_0^{2\pi} e^{i\ell\theta \cos\varphi} d\varphi. \quad (\text{A9})$$

Substituting

$$\int_0^{2\pi} e^{i\ell\theta \cos\varphi} d\varphi = 2\pi J_0(\ell\theta), \quad (\text{A10})$$

we arrive at the well-known result,

$$\xi_+(\boldsymbol{\theta}) = \int_0^\infty \frac{\ell d\ell}{2\pi} J_0(\ell\theta) P_\kappa(\ell). \quad (\text{A11})$$

Similarly, we obtain

$$\xi_-(\boldsymbol{\theta}) = \int_0^\infty \frac{\ell d\ell}{2\pi} J_4(\ell\theta) P_\kappa(\ell). \quad (\text{A12})$$

This paper has been typeset from a $\text{\TeX}/\text{\LaTeX}$ file prepared by the author.